Radiation-pressure-induced nonlinearity in microdroplets

Peng Zhang and Sunghwan Jung*
Department of Biomedical Engineering and Mechanics, Virginia Tech, Blacksburg, Virginia 24061, USA

Aram Lee and Yong Xu†
Department of Electrical and Computer Engineering, Virginia Tech, Blacksburg, Virginia 24061, USA
(Received 4 October 2015; published 31 December 2015)

High quality (Q) factor whispering gallery modes (WGMs) can induce nonlinear effects in liquid droplets through mechanisms such as radiation pressure, Kerr nonlinearity, and thermal effects. However, such nonlinear effects, especially those due to radiation pressure, have yet to be thoroughly investigated and compared in the literature. In this study, we present an analytical approach that can exactly calculate the droplet deformation induced by the radiation pressure. The accuracy of the analytical approach is confirmed through numerical analyses based on the boundary element method. We show that the nonlinear optofluidic effect induced by the radiation pressure is stronger than the Kerr effect and the thermal effect under a large variety of realistic conditions. Using liquids with ultralow and experimentally attainable interfacial tension, we further confirm the prediction that it may only take a few photons to produce measurable WGM resonance shift through radiation-pressure-induced droplet deformation.

DOI: 10.1103/PhysRevE.92.063033 PACS number(s): 47.55.D−, 47.11.Hj

I. INTRODUCTION

Optical whispering gallery modes (WGMs) in dielectric microspheres have been extensively investigated for various applications such as quantum electrodynamics [1] and chemical and biological sensing [2,3]. Due to the high quality factor (Q factor) and small mode volume of WGMs, many nonlinear optical effects can be significantly enhanced in such resonators [4–6]. While most existing research used solid structures as WGM resonators, it has been shown that a microsized liquid droplet immersed in a fluid with lower index can also serve as a good optical resonator [7,8].

During the past decade, there has been significant development in the field of optofluidics, where one used fluids to achieve various optical functionalities such as lasing [9], sensing [3], and tunable photonic devices [10]. Optical techniques have also been used in the characterization of liquid properties [11,12]. The mechanical interplay between optical fields and solid structures has been widely explored in the context of optomechanics [13–16]. By contrast, the impact of optical force on fluidic systems have only been investigated in a limited number of cases [17–23]. In general, optical fields can interact with the fluid system through radiation pressure, scattering force, or thermal capillary force. Ashkin *et al.* [17] first demonstrated that a flat liquid surface can be deformed using focused laser pulses. Later experiments on flat and spherical fluid interfaces with different fluid properties confirmed the effect of radiation pressure on fluid interfaces [18,20–23]. Brasselet *et al.* [22], for example, showed that a stable liquid column can be generated and sustained by the radiation pressure on a system with ultralow interfacial tension ($\sim 1.75 \times 10^{-7}$ N/m). Theoretical and boundary element models were developed to study fluid motion and interface deformations of a flat fluid interface produced by the radiation pressure [20,24]. For liquid droplets, analytical theories were also developed to predict the radiation-pressure effect [19,25–27]. A theoretical description of the droplet shape dynamics was developed in the aforementioned work to quantify the effect of radiation pressure on the drop interface. In a recent work [28], large droplet deformation under optical pressure was also predicted numerically when low interfacial tension was assumed ($\sim 1 \times 10^{-6}$ N/m).

Most research to date analyzed the interplay between optical fields and liquids in isolation and did not consider them as a single coupled system. For example, Refs. [19,20,25–27] investigated the deformation of liquid systems due to the radiation pressure of a focused laser beam. The impact of the deformed liquid systems on the optical fields, however, was not considered. In a recent work [29], we first considered optical fields and liquids as a single system coupled together through optical radiation pressure. Under such a framework, we predict many interesting phenomena such as optofluidic solitons and single-photon-level nonlinearity. In particular, we demonstrated that the existence of radiation pressure on microsized droplets can lead to a large WGM resonance shift that is analogous to the Kerr effect, which is a classical third-order nonlinear process. However, our previous analysis in [29] was based on several approximations. The validity of these approximations was not justified through rigorous analyses. Additionally, the exact shape of the deformed droplet was not obtained.

A major objective of this work is to present an analytical framework that can exactly calculate the deformation of the droplets induced by the radiation pressure of the WGMs. The validity of this analytical method shall be confirmed through direct comparison with numerical fluid simulations based on the boundary element method. The results of our analytical and numerical calculations can also be used to justify the approximation we made in [29]. Additionally, in this study, we quantify the magnitudes of nonlinearities associated with the thermal and Kerr effects, as well as the optofluidic effect induced by the radiation pressure. Specifically, in Sec. II,

*sunnyjsh@vt.edu
†yong@vt.edu

deformations of the droplet interface are solved analytically by force balance on the interface and numerically by the boundary element method (BEM). Section III discusses the thermal effects of the WGM on the refractive index and droplet volume using the BEM. Nonlinearities associated with droplet interface deformation and thermal and Kerr effects are compared in Sec. IV. Finally, the effect of fluid interface tension and the feasibility of single-photon-level nonlinearities are analyzed in Sec. V.

II. RADIATION-PRESSURE-INDUCED DROPLET DEFORMATION

A. WGM in a droplet

We consider a high-Q WGM circulating along the equator of a high-index liquid droplet (core) immersed in a low-index immiscible fluid (cladding). For a typical drop, its radius a is of the order of 100 μm, and the density difference $\Delta\rho$ between two fluids is about 200 kg/m^3. Such an optofluidic system possesses a low Bond number ($\mathrm{Bo} = \Delta\rho g a^2/\sigma \sim 10^{-3}$, where the surface tension $\sigma \sim 30$ mN/m) and a low Reynolds number ($\mathrm{Re} = \rho U a/\mu \sim 10^{-2}$, where the characteristic velocity $U = 10^{-3}$ m/s and fluid viscosity $\mu = 13$ mPa s). Given the low Bond and Reynolds numbers, we can safely ignore gravity and inertia effects in our analysis. In this paper, we denote variables associated with the core phase with subscript "co" and the cladding phase with subscript "cl".

To simplify our analysis, the optical field in the resonator is assumed to be a transverse electric (TE) mode, which can be expressed as [30]

$$\begin{aligned} \vec{E}_{lm} &= g_l(kr)\vec{X}_{lm}(\theta,\phi), \\ \vec{H}_{lm} &= -\frac{i}{kZ}\vec{\nabla}\times[g_l(kr)\vec{X}_{lm}(\theta,\phi)], \end{aligned} \tag{1}$$

where mode numbers l and m satisfy $l > 0$, $-l \leqslant m \leqslant l$; ω and k are the frequency and wave number, respectively, of the WGM, where $k = k_{\mathrm{co}} = \omega_{\mathrm{co}}/c$ in the droplet core and $k = k_{\mathrm{cl}} = \omega_{\mathrm{cl}}/c$ in the cladding region; Z is the impedance of the liquid; $\vec{X}_{lm}(\theta,\phi)$ is the vector spherical harmonic function; $g_l(kr)$ is either the spherical Bessel function (if in the core phase) or the spherical Hankel function (if in the cladding phase),

$$g_l(kr) = \begin{cases} A_{\mathrm{co}} j_l(k_{\mathrm{co}} r), & r \leqslant a, \\ A_{\mathrm{cl}} h_l^{(1)}(k_{\mathrm{cl}} r), & r > a, \end{cases} \tag{2}$$

where A_{co} and A_{cl} are two constants to be determined by matching the optical field across the drop interface. The field-matching process also gives the frequency ω of the WGM. We denote the WGM in Eq. (1) as $|l,m\rangle$. Once the WGM frequency is known, we can readily determine the field distribution of the WGM using Eqs. (1) and (2). For more details, refer to Ref. [29]. In this paper, we are primarily interested in the fundamental WGM with $l = m \gg 1$, which corresponds to a high-Q WGM circulating along the droplet equator, as illustrated in Fig. 1.

As demonstrated in [29] and illustrated in Fig. 1, the radiation pressure of the WGM can deform the liquid resonator and produce a large shift in the WGM resonance frequency.

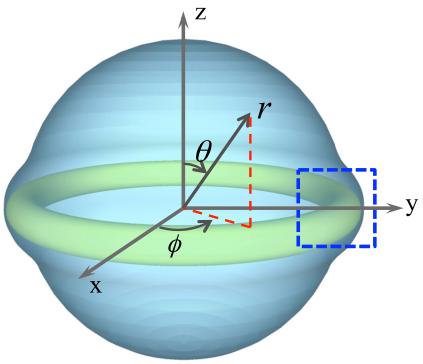

FIG. 1. (Color online) Schematic of a droplet containing a high-Q WGM circulating along the equator with a deformed interface. A spherical coordinate system (r,θ,ϕ) is defined to assist further analysis.

The radiation pressure of the WGM can be calculated as [29]

$$p_{\mathrm{opt}} = \tfrac{1}{2}\epsilon_0\left(n_{\mathrm{co}}^2 - n_{\mathrm{cl}}^2\right)|\vec{E}_{\mathrm{surf}}|^2, \tag{3}$$

where ϵ_0 is the free space permittivity, n_{co} and n_{cl} are refractive indices of the liquid core and cladding, respectively, and $\vec{E}_{\mathrm{surf}}$ is the electric field on the interface. Given the expression in Eq. (3), the radiation pressure p_{opt} of the WGM is proportional to the total circulating power (P_{WGM}) associated with the WGM. As in [29], P_{WGM} can be calculated through a surface integration of the Poynting vector component S_ϕ over a cross section on any $\phi =$ constant plane (as shown by the dashed rectangle in Fig. 1),

$$P_{\mathrm{WGM}} = \iint S_\phi dA. \tag{4}$$

In Secs. II B and II C, we describe two different approaches that can calculate the interface deformation and fluid motions induced by the radiation pressure on the droplet.

B. Balanced interface shape

On a stationary fluid interface, the forces on the interface must be balanced by the interfacial tension. When the optical radiation pressure is applied on the interface, the Young-Laplace equation implies

$$\sigma\vec{\nabla}\cdot\hat{n} = p_{\mathrm{co}} - p_{\mathrm{cl}} + p_{\mathrm{opt}}, \tag{5}$$

where σ is the interfacial tension and $\hat{n}$ is the unit normal vector to the surface. Bulk pressures in the core and cladding phases are $p_{\mathrm{co}} = p_{\mathrm{co}}^0 + \Delta p$ and $p_{\mathrm{cl}} = p_{\mathrm{cl}}^0$, respectively. Here, p_{co}^0 and p_{cl}^0 are equilibrium pressures in the core and cladding phases before deformation, which satisfy $2\sigma/a = p_{\mathrm{co}}^0 - p_{\mathrm{cl}}^0$. Δp is the pressure increase inside the droplet caused by the optical pressure, which is determined later. The Young-Laplace equation for a spherical droplet with the radiation pressure becomes

$$\sigma\vec{\nabla}\cdot\hat{n} = \sigma\frac{2}{a} + \Delta p + p_{\mathrm{opt}}. \tag{6}$$

Assuming axial symmetry and using spherical coordinates, we can describe the interface shape as $r(\theta) = a + \Delta R(\theta)$, where $\Delta R(\theta)$ is the interface deformation. Hence, the interface

curvature ($\vec{\nabla}\cdot\hat{n}$) can be calculated based on the form of $\Delta R(\theta)$. We can further normalize the shape deformation by a as $h(\theta)=\Delta R(\theta)/a$. Under the assumption of small deformation ($h\ll 1$), the Young-Laplace equation (6) is linearized as

$$h''(\theta)+\cot(\theta)h'(\theta)+2h(\theta)=-\frac{a}{\sigma}(\Delta p+p_{\rm opt}). \quad (7)$$

The unknown Δp value in Eq. (7) serves as a Lagrange multiplier to ensure the volume conservation of droplet. For a given trial value of Δp, Eq. (7) is integrated numerically to produce a solution $h(\theta)$, from which the droplet volume is calculated. Among all the trial values of Δp, the only Δp that satisfies the conservation of the droplet volume is assumed to be the true value.

Due to the linearity of Eq. (7), it is clear that $h(\theta)$ is proportional to $1/\sigma$ and the magnitude of $p_{\rm opt}$ ($\propto P_{\rm WGM}$) (see Appendix A). This relation holds as long as the small deformation assumption is valid.

C. Boundary element method

The motions of the fluid interface and volume are governed by the Navier-Stokes equations. Stokes equations can be applied to this problem as a consequence of the low Reynolds number. Stokes equations and incompressibility condition are written as

$$-\vec{\nabla}p+\mu\nabla^2\vec{u}=0,\quad \vec{\nabla}\cdot\vec{u}=0. \quad (8)$$

Stokes equations can be solved numerically by the BEM [31]. For a two-phase fluid system with a sharp interface, the interfacial velocity and pressure are related by the following boundary integral equations,

$$\vec{u}(\vec{x}_0)=-\frac{1}{4\pi\mu_{\rm cl}(1+\lambda)}\int_S(\sigma\vec{\nabla}\cdot\hat{n}-p_{\rm opt})\hat{n}\cdot\boldsymbol{U}(\vec{x}_0,\vec{x})\times dS(\vec{x})+\frac{(1-\lambda)}{4\pi(1+\lambda)}\int_S\vec{u}(\vec{x})\cdot\boldsymbol{K}(\vec{x}_0,\vec{x})\cdot\hat{n}(\vec{x})\,dS(\vec{x}), \quad (9)$$

where $\lambda=\mu_{\rm co}/\mu_{\rm cl}$ is the viscosity ratio of the core and cladding phases; "S" denotes the interface of the droplet; and position vectors $\vec{x}$ and $\vec{x}_0$ are located on the fluid interface. Also, $\boldsymbol{U}$ and $\boldsymbol{K}$ are Green's functions for Stokes flow in free space,

$$\boldsymbol{U}(\vec{x},\vec{y})=\frac{1}{d}\boldsymbol{I}+\frac{1}{d^3}\vec{d}\vec{d},\ \boldsymbol{K}(\vec{x},\vec{y})=-\frac{6}{d^5}\vec{d}\vec{d}\vec{d}, \quad (10)$$

with $\vec{d}=\vec{x}-\vec{y}$, $d=|\vec{x}-\vec{y}|$, and $\boldsymbol{I}$ is the identity tensor.

Due to the axisymmetric nature of the geometry and boundary conditions, we can integrate Eq. (9) over the ϕ variable analytically to simplify the numerical implementation. The resulting boundary integral equations and Green's functions are well known and available in literature [31,32].

In our simulations, the fluid interface on the $\phi=$ constant plane is discretized into N circular arc elements, and $\vec{x}_0$ are located at the center of each element. Assuming constant surface velocity and pressure on each element, Eq. (9) can be discretized and written as a linear system relating the unknown interface velocity ($\{v_i\}$) and the known pressure ($\{f_i\}=(\sigma\vec{\nabla}\cdot\hat{n}-p_{\rm opt})\{\hat{n}_i\}$) vectors,

$$A_{ij}v_j=B_{ij}f_j, \quad (11)$$

where $[A_{ij}]$ and $[B_{ij}]$ are $2N\times 2N$ matrices whose entries are integrals of $\boldsymbol{U}$ and $\boldsymbol{K}$ on the interface elements.

The solution to the above linear system gives the velocity at the center of each element on the interface. Velocities at the end points of each element are interpolated by a cubic spline with vanishing derivatives at $\theta=0,\pi$. The element edges and center displacements are integrated over time by an explicit Euler scheme, i.e., $\Delta\vec{x}=\vec{u}\Delta t$, and a new interface shape is obtained for the following time step. The time step size is chosen by the criteria $\Delta t\leqslant\tau_m=(\mu_{\rm co}+\mu_{\rm cl})l/(2\sigma)$, where l is the element size [33]. This process is iterated until the maximum velocity magnitude $|\vec{u}|$ is sufficiently small.

In our simulations, we find that $N=128$ elements are sufficient to resolve the interface shape. Each numerical simulation takes about 10–12 h of CPU time until a convergent interface shape is obtained.

III. THERMAL NONLINEARITY

The optical power ($P_{\rm WGM}$) carried by the WGM in the resonator can possibly be absorbed by the liquid and converted into thermal energy. Therefore, the droplet temperature may change, which should lead to changes in the optical properties of the droplet as well as the WGM. In this section, we provide an order of magnitude estimate on the thermal effects.

First, we define the steady-state temperature change (T) as the temperature variation induced by the WGM energy. The spatial variation of T in the liquid, which is induced by a heat flux associated with the absorption of the WGM, is governed by the Poisson equation

$$\nabla^2T(\vec{x})=g(\vec{x}), \quad (12)$$

where $g(\vec{x})=-\alpha S_\phi/\kappa_{\rm co}$ [34], α is the absorption constant of the droplet core, and $\kappa_{\rm co}$ is the thermal conductivity of the core liquid. Here we assume that optical absorption occurs predominantly in the droplet core, and all absorbed optical energy is converted to heat.

The solution of temperature field within the droplet core can be easily obtained from the results in [30]

$$T(\vec{x}_0)=-\int_V g(\vec{x})G(\vec{x},\vec{x}_0)dV(\vec{x})-\int_S G(\vec{x},\vec{x}_0)[\hat{n}(\vec{x})\cdot\vec{\nabla}T(\vec{x})]dS(\vec{x})+\int_S T(\vec{x})[\hat{n}(\vec{x})\cdot\vec{\nabla}G(\vec{x},\vec{x}_0)]dS(\vec{x}), \quad (13)$$

where $G=1/(4\pi|\vec{x}-\vec{x}_0|)$ is the free space Green's function and "V" denotes the core fluid volume. The temperature change in the cladding phase is also governed by Eq. (13) with corresponding fluid properties.

In our simulations, we assume the continuity of temperature and heat flux at the droplet interface. We also assume that in the cladding region far away from the droplet, liquid temperature remains unchanged. Similar to the techniques used in Sec. II C, we also take advantage of the axisymmetry of the problem and introduce a discretization of the boundary on the

ϕ = constant plane. We can then relate the discretized interface temperature values ($\{T_i\}$) to the known volume integral ($\{I_i^v\}$) at the boundary elements by a linear system similar to Eq. (11),

$$H_{ij}T_j = I_i^v, \tag{14}$$

where $[H_{ij}]$ is an $N \times N$ matrix whose entries are integrals of the Green's function on the interface elements.

The thermally induced refractive index change (denoted as Δn_T) can be estimated by

$$\Delta n_T = \frac{dn}{dT} T_{\max}, \tag{15}$$

where (dn/dT) is the thermal coefficient of refractive index and $T_{\max}$ is the maximum temperature change in the droplet.

The droplet may also expand in size as its temperature increases. To estimate the effect of thermal expansion, we consider the change in droplet radius near its equator, $\Delta R_T \equiv \Delta R(\theta = \pi/2)/a$. To simplify our analysis, we "overestimate" its magnitude by assuming that the mode volume of the WGM is uniformly heated to the maximum temperature within the droplet ($T_{\max}$). The relative change of radius is then

$$\Delta R_T = \tfrac{1}{3}\alpha_T T_{\max}, \tag{16}$$

where α_T is the thermal expansion coefficient.

IV. NONLINEAR EFFECTS IN LIQUID DROPLETS

The properties of the WGMs depend on the liquid refractive indices as well as the size and shape of the resonator. In our studies of nonlinear effects, we choose a liquid system based on an oil droplet immersed in water. The fluid we used for the droplet core is an index-matching fluid (Series AA14500, Cargille Laboratories). Fluid viscosities of the core and cladding media are $\mu_{co} = 13$ mPa s and $\mu_{cl} = 1$ mPa s, and the heat conductivities are $\kappa_{co} = 0.126$ W/m K and $\kappa_{cl} = 0.60$ W/m K, respectively. The oil-water interfacial tension is measured by a goniometer (Model 590, ramé-hart instrument co.) to be around $\sigma = 30$ mPa s.

This system has the highest Q factor at the wavelength of $\lambda \approx 700$ nm, since optical absorption is lowest at this wavelength. At $\lambda \approx 700$ nm, the effective refractive indices of the core and cladding phases are $n_{co} = 1.44$ and $n_{cl} = 1.33$, respectively. We apply the procedure in [29] to determine the resonance frequency of the WGMs resonator. We first consider the fundamental mode $|l,l\rangle$, which corresponds to an optical field with a single maximum along the polar direction. The angular mode number l's of the WGMs are chosen so that λ's are close to 700 nm. Table I gives the angular mode number l and the resonance wavelength λ of the WGMs in droplets with different radii a.

TABLE I. Angular mode number l and resonance wavelength λ of WGMs in liquid droplets.

a (μm)	400	300	250	200	150	120
l	5145	3847	3204	2569	1918	1529
λ (nm)	699.35	700.66	700.45	698.05	699.95	701.26
a (μm)	100	80	70	60	50	40
l	1275	1018	889	761	632	504
λ (nm)	699.75	699.65	700.05	699.75	700.55	700.59

Assuming that absorption in the droplet core is the only source of the energy loss, we can estimate the WGM Q factors of the above resonators to be $Q = 2\pi n_{co}/(\alpha\lambda) \approx 10^8$ with absorption constant $\alpha = 0.125$ m^{-1} (according to the specification of the index-matching fluid). The interface deformations of the above resonators are computed using both the analytical method in Sec. II B and the numerical method in Sec. II C. Nonlinearities due to interface deformation, temperature change, and Kerr effect are estimated separately.

A. Nonlinear effects

In this section, we consider nonlinearities associated with the fundamental WGM $|l,l\rangle$, with the mode number l given by Table I. The electric field across the droplet interface is calculated by Eq. (1). As an example, the electric field intensity in a droplet with $a = 100$ μm is shown in Fig. 2. The total WGM power of the electric field is then given by Eq. (4). Since nonlinear effects induced by the radiation pressure are proportional to P_{WGM}, we only need to analyze droplet deformation at a specific WGM power level. In this paper, the electric field is normalized such that the total WGM power is $P_{WGM} = 1$ W. With known electric field intensity on the interface, droplet interface deformations induced by the radiation pressure are computed by the force balance Eq. (7) and BEM Eq. (9).

In Fig. 3, we compare the interface deformation obtained using the analytical method in Sec. II B and the numerical BEM simulations described in Sec. II C. The equilibrium interface shapes obtained by the BEM are in excellent agreement with the force balance predictions given by Eq. (7). The BEM solutions also produce a velocity distribution in the droplet, as shown in Fig. 4.

As discussed in Sec. II B, the maximum droplet interface deformation $\Delta R/a$ is linearly dependent on the values of $1/\sigma$ and P_{WGM}, which is also implied by the approximated solution in literature [29] [Sec. IV B, Eq. (17)]. Therefore, the interface

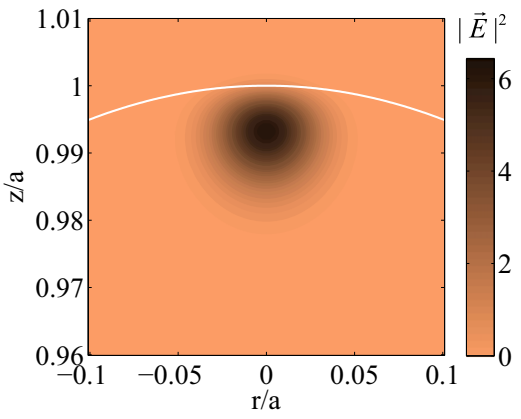

FIG. 2. (Color online) $|\vec{E}|^2$ distribution in the droplet on a ϕ = constant plane. The electric field has been normalized so that on the interface the maximum intensity $|\vec{E}|^2_{\max} = 1$. The white curve represents the droplet interface.

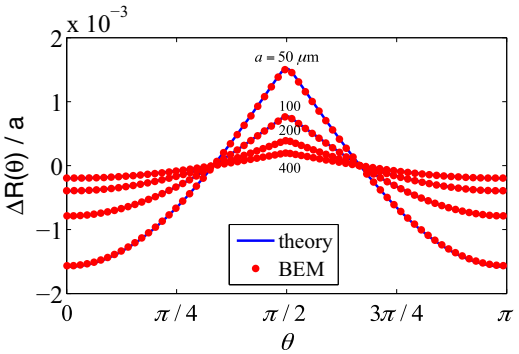

FIG. 3. (Color online) Solutions of the balanced interface deformation by the Young-Laplace equation and the BEM simulations for radii $a = 50$, 100, 200, and 400 μm.

shapes under arbitrary WGM powers and interfacial tension values can be linearly extrapolated from the solutions in Fig. 3.

The temperature change due to the optical absorption of the WGM can be computed numerically as described in Sec. III. Again, we assume that the circulating WGM power is 1 W and that all optical energy absorbed by the core liquid ($\alpha = 0.125$) is converted to heat. Based on Eqs. (12) to (14), we can calculate temperature distribution within the droplet. The results are shown in Fig. 5. Figure 6 gives the changes in refractive index and the size of the liquid core as estimated by Eqs. (15) and (16), where we assume the core liquid possesses a thermal coefficient of $(dn/dT) = -3.9 \times 10^{-4}$ K^{-1}, and a thermal expansion coefficient of $\alpha_T = 8 \times 10^{-4}$ K^{-1}. In terms of their impact on the WGMs, these two thermal processes are nearly the same, as can be seen from Fig. 6.

Kerr effect is a classical third-order nonlinear process, where the material refractive index depends linearly on optical field intensity [35]. For the liquid resonator, the refractive index change as a result of the Kerr effect can be estimated as $\Delta n \approx \chi^{(3)} |\vec{E}|^2_{\max}$, where $\chi^{(3)}$ is the third-order nonlinear optical susceptibility and $|\vec{E}|_{\max}$ is the maximum electric field intensity in the droplet. To provide an order of magnitude estimate of the Kerr effect, we use water and carbon disulfide (CS_2) ($\chi^{(3)}_{\text{water}} = 2.5 \times 10^{-22}$ m^2/V^2 and $\chi^{(3)}_{CS_2} = 3.1 \times 10^{-20}$ m^2/V^2) to calculate the refractive index change.

We now compare the impact of the three nonlinear processes—radiation pressure effect, thermal effects, and Kerr

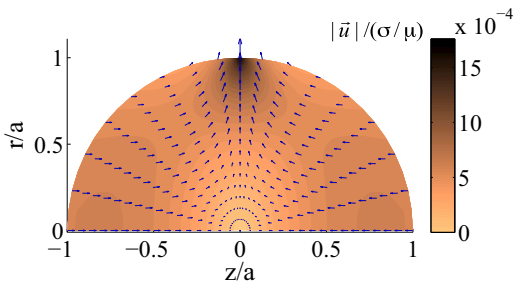

FIG. 4. (Color online) Fluid velocity direction (arrows) and magnitude (color) distribution on the $x = 0$ plane at time $t = 0$. Velocity values are normalized by σ/μ.

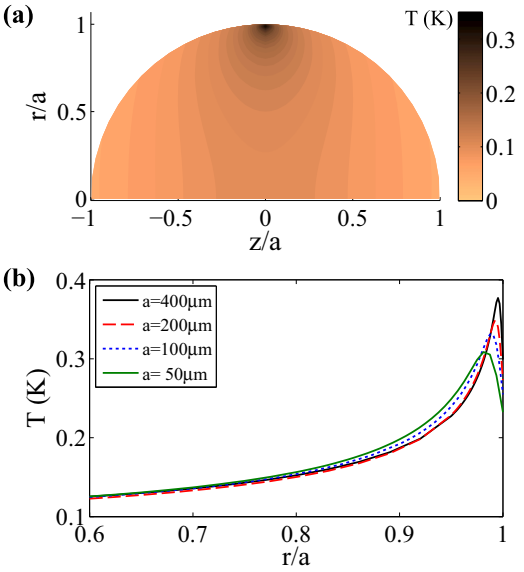

FIG. 5. (Color online) Changes in fluid temperature in the liquid core due to optical absorption. (a) Temperature distribution in the $x = 0$ plane for a droplet with radius $a = 100$ μm. (b) Radial temperature distribution at $\theta = \pi/2$ for droplets with radii $a = 50$, 100, 200, and 400 μm.

effect—on liquid droplets. Let us define the interface deformation at the equator as $\Delta R(\theta = \pi/2)/a \equiv \Delta R_p$. As shown in Fig. 6, interface deformation induced by the radiation pressure (ΔR_p) is a few orders of magnitude higher than the Kerr effect ($\Delta n/n$). Additionally, for smaller liquid droplets, nonlinearity caused by the radiation pressure is also significantly higher than the thermal nonlinearity. However, for millimeter-sized droplets, the radiation-pressure effect and the thermal effects can be comparable in magnitude. However, even for cases where thermal effects are significant, it might be possible

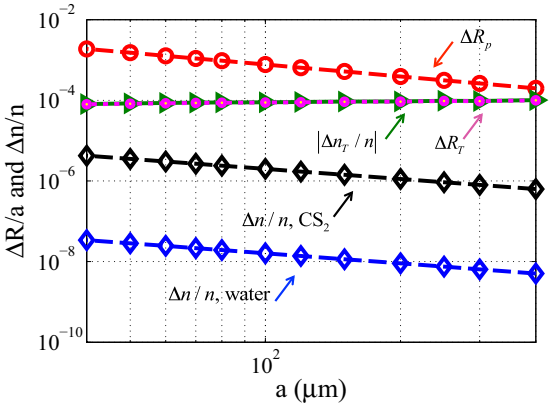

FIG. 6. (Color online) Comparison of the strength of nonlinearity due to radiation pressure, thermal effects, and Kerr effect. The vertical axis is either relative deformation at the droplet equator [$\Delta R(\theta = \pi/2)/a$, caused by radiation pressure and thermal expansion] or refractive index changes ($\Delta n/n$, caused by thermo-optic effect and Kerr nonlinearity). Droplet radius changes ΔR_T associated with thermal expansion overlap with the refractive index changes $\Delta n_T/n$ induced by temperature changes.

to distinguish radiation-pressure effect and thermal effects through direct measurements of the interface deformation. According to Fig. 6, for a droplet with 100 μm radius and typical interfacial tension ($\sigma = 30$ mN/m), a WGM with 1 W power can deform the droplet radius by approximately 100 nm. Many optical interferometry techniques are capable of measuring this estimated interfacial deformation. For example, the methods reported in Refs. [36–38] can all measure surface deformation with nanometer or subnanometer spatial resolutions.

B. Comparison of the exact solution and the approximate solution

In [29], we gave an analytical formula that can estimate the magnitude of the nonlinearity induced by the radiation pressure. In that approach, the droplet deformation was approximated by an ellipsoid and the radius change at the equator $[\Delta R(\theta = \pi/2)/a]$ was given by

$$\Delta R_p = \frac{\Gamma_\theta^{lm}\epsilon_0\lambda}{4\Gamma_\sigma\sigma n_{\rm co}}\left(n_{\rm co}^2 - n_{\rm cl}^2\right)\left|\vec{E}_{\rm surf}^{\rm peak}\right|^2, \tag{17}$$

where $\Gamma_\sigma \approx 1.01$ is given by the ellipsoid assumption and Γ_θ^{lm} is associated with the angular dependence of the radiation pressure,

$$\Gamma_\theta^{lm} = -\frac{n_{\rm co}a}{\lambda}\int_0^\pi f_{lm}Y_{20}(\theta)\sin(\theta)\,d\theta, \tag{18}$$

where f_{lm} is the normalized radiation pressure whose maximum value on the interface is one.

With the help of Clebsch-Gordan coefficients, Eq. (18) can be simplified as (Appendix B),

$$\Gamma_\theta^{lm} = -\frac{n_{\rm co}a}{\lambda}\frac{1}{2\pi|\vec{X}_{lm}|_{\rm max}^2}\left[1 - \frac{3}{l(l+1)}\right]\sqrt{\frac{5}{4\pi}} \times \langle 2,l;0,m|l,m\rangle\langle 2,l;0,0|l,0\rangle. \tag{19}$$

Note that, taken together, Eqs. (17) and (19) give an analytical estimate for the droplet deformation induced by the radiation pressure. The accuracy of this analytical approximation is investigated here.

The exact interface deformation can be expressed in terms of the spherical harmonics Y_{LM} as

$$\frac{\Delta R(\theta)}{a} = \sum_{L=2}^{N}\sqrt{4\pi}\,\Delta_L Y_{L0}(\theta), \tag{20a}$$

$$\frac{\Delta R(\pi/2)}{a} = \sum_{L=2}^{N}(\Delta R_p)_L, \tag{20b}$$

where $Y_{L0}(\theta)$ is the spherical harmonic function $Y_{L0}(\theta,\phi)$ with $\phi = 0$, Δ_L is the expansion coefficient, and $(\Delta R_p)_L = \sqrt{4\pi}\,\Delta_L Y_{L0}(\pi/2)$ denotes droplet deformation at the equator due to the Y_{L0} term. Due to the rotational symmetry (with respect to the z axis) and the mirror reflection symmetry (with respect to the $z = 0$ plane), the droplet deformation does not contain any Y_{LM} term with odd L number or with $M \neq 0$. The values of $(\Delta R_p)_L$ up to $L = 50$ are shown in Fig. 7 for interface deformations of droplets with four different radii. Note that we must have $(\Delta R_p)_0 = 0$ to satisfy the volume conservation. Figure 7 shows that the value of $|(\Delta R_p)_L|$ decreases rapidly as L increases, with $(\Delta R_p)_2$ being the dominant term. A comparison of the $L = 2$ term in Fig. 7 with the solution in Eq. (17) is shown in Table II. In Fig. 8(a), we also compare the exact droplet deformation given by the current work with the approximate solution in Eq. (17). The results show that the first-order approximation in Eq. (17) can provide a reasonably accurate prediction of the interface deformation caused by the radiation pressure. In fact, if we change the constant Γ_σ in Eq. (17) from $\Gamma_\sigma = 1.01$ to $\Gamma_\sigma = 0.643$, the slightly modified analytical formula ["modified approx." in Fig. 8(a)] agrees very well with the equator deformation ΔR_p as given by the exact solutions. This excellent agreement can be explained by the observation that for the simulation parameters considered in this work, the interfacial deformation $\Delta R(\theta)/a$ can be factored into a product of the equator deformation ΔR_p and an angular shape function $f(\theta)$, with $f(\theta)$ being mostly independent of parameters such as droplet radius, interfacial tension, and optical power. This observation can be easily confirmed by normalizing various orders of $(\Delta R_p)_L$ with the leading term $(\Delta R_p)_2$, as shown in Fig. 8(b). Regardless of droplet radius, the normalized deformation factors, $(\Delta R_p)_L/(\Delta R_p)_2$, are almost identical, which indirectly confirms the shape independence of the radiation-pressure-induced deformation.

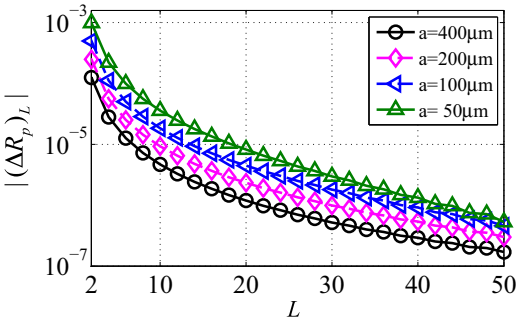

FIG. 7. (Color online) Spherical harmonics expanded terms $[|(\Delta R_p)_L|]$ in Eq. (20b) for four cases shown in Table I. Coefficients with odd indices are zero and are not shown here.

V. SINGLE-PHOTON-LEVEL NONLINEARITY

In this section, we discuss perhaps the most important prediction of our theoretical analysis, namely the feasibility of single-photon-level nonlinearity.

As proposed in [29], for the ultralow interfacial tension fluid systems that have been demonstrated in the past experiments,

TABLE II. The approximate analytic solutions of droplet deformation [ΔR_p according to Eq. (17)] and the leading spherical harmonic expansion term [$(\Delta R_p)_2$, due to Y_{20} only] of the exact interface deformation solution.

a (μm)	ΔR_p	$(\Delta R_p)_2$
400	1.247×10^{-4}	1.246×10^{-4}
200	2.490×10^{-4}	2.488×10^{-4}
100	4.967×10^{-4}	4.962×10^{-4}
50	9.891×10^{-4}	9.882×10^{-4}

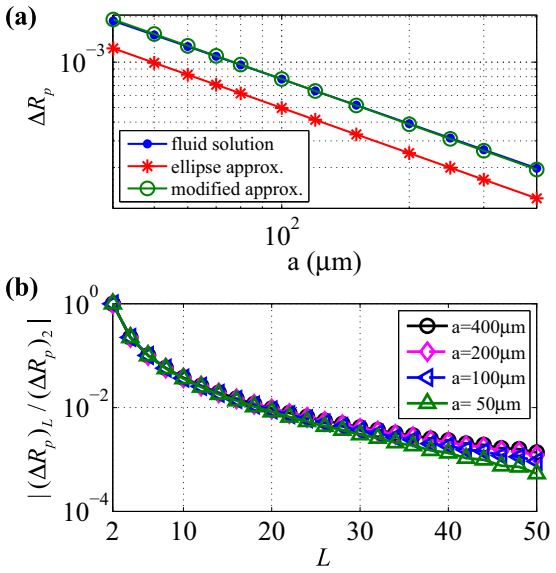

FIG. 8. (Color online) (a) Comparison of the maximum interface deformation between exact solutions given by the current work with approximated solutions in [29]. (b) Spherical harmonics expanded terms $[|(\Delta R_p)_L|]$ normalized by the first nonzero term $|(\Delta R_p)_2|$.

the radiation-pressure-induced droplet deformation may lead to a measurable WGM shift at the single-photon energy level. In contrast with our earlier work [29] based on the approximate solution, here we estimate the magnitude of the WGM resonance shift induced by the radiation pressure using the exact solution presented in Sec. IV.

The general framework of our analysis is as follows. First, we expand the exact solution of the deformed droplet using spherical harmonic functions. Then, based on the perturbation theory in [39], we can sum over the frequency shift due to each spherical harmonic term and obtain the total resonance shift for a specific WGM mode $|l,m\rangle$. Mathematically, this means

$$\frac{\Delta\omega}{\omega}=\sum_{L=2,4,6,\ldots}^{\infty}\frac{\Delta\omega_L}{\omega}=-\sum_{L=2,4,6,\ldots}^{\infty}\Delta_L F(L,l,m), \qquad (21)$$

where the expansion coefficients Δ_L are given in Eq. (20a), and $F(L,l,m)$ can be derived as

$$\begin{aligned}F(L,l,m)&=\sqrt{4\pi}\iint|\vec{X}_{lm}|^2Y_{LM}\,d\Omega\\&=\left[1-\frac{L(L+1)}{2l(l+1)}\right]\sqrt{2L+1}\\&\quad\times\langle L,l;M,m|l,m\rangle\langle L,l;0,0|l,0\rangle. \qquad (22)\end{aligned}$$

The expression in Eq. (22) is derived in Appendix B. Values of $|(\Delta\omega_L/\omega)/(\Delta\omega_2/\omega)|$ up to $L=50$ in Eq. (21) are shown in Fig. 9 for several representative cases. Clearly, the leading contribution is due to the lowest-order deformation (i.e., the $L=2$ term).

As proposed in [29], droplet deformation due to a single photon can occur if fluids with low interfacial tensions are used. The WGM frequency shifts induced by the interface deformation as a result of WGM with single-photon energy ($\hbar\omega$) are shown in Fig. 10. Terms up to $L=200$ are considered

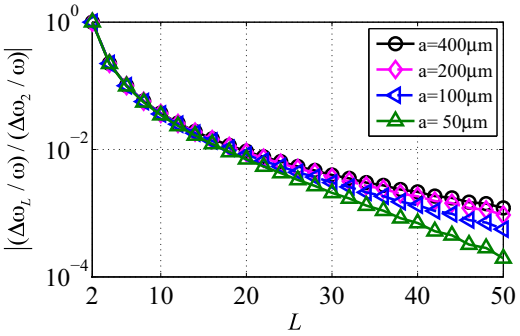

FIG. 9. (Color online) Contribution to WGM frequency shift as a result of different Y_{LM} terms in shape deformation $\Delta\omega_L/\omega$ in Eq. (21), normalized by the leading contribution $\Delta\omega_2/\omega$.

in the summation (21). The results for a lower interfacial tension assumption ($\sigma=1$ mN/m) are also shown in the same plot. The solid lines in Fig. 10 correspond to the exact solutions given by Eq. (21), whereas the dashed lines are based on the approximate solutions in [29]. The frequency shifts given by the exact solution are actually larger than our original estimates given in [29]. Experimentally, frequency shift as small as $\Delta\omega/\omega\sim10^{-8}$ has been measured [40]. Based on this value and the results shown in Fig. 10, it should be feasible to detect the frequency shift induced by a single photon if the droplet diameter is around 10 μm and the interfacial tension is of the order of $\sigma=1$ mN/m. Again, our results confirm the possibility of optical nonlinearity induced by only a few photons.

It is worth mentioning that droplets with low interfacial tensions ($\sigma\leqslant1$ mN/m) have been obtained in different studies [41–43]. With the help of surfactant, an interfacial tension as low as 1 μN/m was obtained in an emulsion system [44].

To investigate the nonlinear optofluidic effects for higher-order WGMs $|l,m\rangle$ with $m<l$, we also calculate the droplet interface deformations and the frequency changes induced by such modes. The results are shown in Fig. 11 as blue (dark gray) bars, which give the frequency shifts of the $|l,m\rangle$ mode. For these results, the radiation pressure is produced by

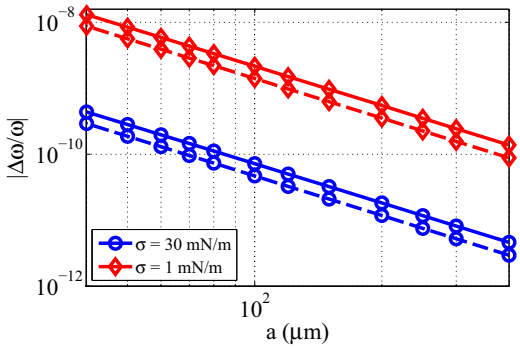

FIG. 10. (Color online) WGM frequency shift induced by the radiation pressure of a single photon for interfacial tension $\sigma=30$ mN/m and $\sigma=1$ mN/m. Solid lines are the frequency shift values computed by the exact interface shape, while dashed lines are computed from the first-order approximated interface deformation.

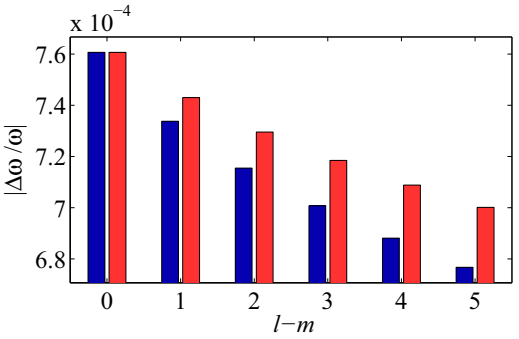

FIG. 11. (Color online) Resonance frequency shift in a droplet with radius $a = 100\ \mu$m and interfacial tension $\sigma = 30$ mN/m for WGMs $|l,m\rangle$ with the same $l = 1275$ but different m numbers. The blue (dark gray) bars give the frequency shifts of the $|l,m\rangle$ mode that is caused by the radiation pressure of itself, i.e., the $|l,m\rangle$ mode. The red (light gray) bars are the frequency shift of the $|l,m\rangle$ mode, where radiation pressure is produced by the fundamental mode $|l,l\rangle$.

the $|l,m\rangle$ mode itself. Note that the fundamental mode $|l,l\rangle$ generates the largest frequency shift. Since the droplet is no longer a sphere, the $(2l+1)$-fold degeneracy of the WGM should be broken. To quantify this effect, we also calculate the frequency shifts of the $|l,m\rangle$ mode, where the radiation pressure is produced by the fundamental WGM mode $|l,l\rangle$. The results are again shown in Fig. 11 as red (light gray) bars. As expected, WGMs with the same l but different m numbers are no longer degenerate. All results in Fig. 11 are based on a droplet with radius $a = 100\ \mu$m, with $l = 1275$ and $P_{\mathrm{WGM}} = 1$ W for the WGMs.

In the calculation of the thermal effects, we neglected the thermocapillary effect caused by the temperature increase. To justify this, here we estimate the interfacial tension increase and the resulting shear stress on the interface. Based on the well-known Eötvös rule [45], the interfacial tension of the fluid system is given by $\sigma = \bar{k}(T_c - T)/\bar{V}^{2/3}$, where $\bar{k}$ and $\bar{V}$ are material properties and T_c is the critical temperature of the fluid. Using the critical temperature of water $T_c = 374\,^{\circ}$C and a temperature increase of $1\,^{\circ}$C from room temperature ($25\,^{\circ}$C), the change in interfacial tension is $\Delta\sigma/\sigma = -0.28\%$. Along the arc length of the droplet interface, s, the shear stress is roughly, $\partial\sigma/\partial s \approx 1.8 \times 10^{-3}(\sigma/a)$. Compared with the maximum radiation pressure on the interface of the $a = 100\ \mu$m droplet, $p_{\mathrm{opt}}^{\mathrm{max}} \approx 6 \times 10^{-2}(\sigma/a)$, we have $(\partial\sigma/\partial s)/p_{\mathrm{opt}}^{\mathrm{max}} \approx 3\%$. Thus, the thermocapillary effect can be neglected in our calculations of the interface deformation.

Our calculations on droplets with lower surface tension show that a single photon can possibly produce measurable interfacial deformation. However, recent studies show that the effect of thermal fluctuations may become important for interfaces with low interfacial tension [46,47], and thus it might be difficult to distinguish the single-photon effect from those due to thermal fluctuations. To reduce the effect of thermal fluctuation experimentally, we may consider using liquid drops at low temperature. For example, the surface tension of a liquid helium droplet at temperature $T < 1$ K is $\sigma \sim 0.38$ mN/m [48], which is low enough to admit single-photon nonlinearity.

In summary, this section confirms the feasibility of single-photon-level nonlinearity if the interfacial tension of the liquid droplet is of the order of $\sigma = 1$ mN/m or less. Our results also suggest that radiation-pressure-induced deformation should lift the degeneracy of the WGMs.

VI. CONCLUSION

In this paper, we investigate the nonlinear optofluidic effect in microsized liquid resonators. The nonlinearity is induced by the radiation pressure associated with a high-Q WGM. The interface deformation of the liquid droplet is calculated both analytically by force balance and numerically by BEM, which agree with each other very well. The effect of temperature change is also quantified by BEM. The nonlinearity induced by the radiation pressure is shown to be higher than the temperature effect and the Kerr effect. Based on our analytical and numerical models, we confirm the possibility of measurable optofluidic nonlinearity at the single-photon energy level. The conditions that may allow one to experimentally observe single-photon-level nonlinear optofluidic effects are also discussed. Experimental measurement of the nonlinearity induced by the radiation pressure will be performed using the white light interferometry technique for future research.

ACKNOWLEDGMENTS

This research was supported by the National Science Foundation (Grant No. CBET 1438112).

APPENDIX A: LINEAR RELATION BETWEEN Δp AND p_{opt}

We claim that the value of Δp is proportional to P_{WGM}. To prove this, let us assume a Δp^1 and p_{opt}^1 (corresponding to P_{WGM}^1) result in an interface deformation $h^1(\theta)$ that satisfies Eq. (7) and volume conservation, i.e.,

$$h^{1\prime\prime}(\theta) + \cot(\theta)h^{1\prime}(\theta) + 2h^1(\theta) = -\frac{a}{\sigma}\left(\Delta p^1 + p_{\mathrm{opt}}^1\right). \quad \text{(A1)}$$

If we change the WGM power to $\alpha P_{\mathrm{WGM}}^1$, then the optical pressure will be $\alpha p_{\mathrm{opt}}^1$, where α is a constant. We now show that $\alpha\Delta p^1$ gives a $h(\theta)$ that satisfies volume conservation. If we simply substitute $\alpha\Delta p^1$ and $\alpha p_{\mathrm{opt}}^1$ on the right hand side of Eq. (A1), then the solution to Eq. (A1) should be $\alpha h^1(\theta)$, because of the linearity of Eq. (A1). Since $h^1(\theta)$ give zero volume change, $\alpha h^1(\theta)$ should also preserve the volume. Therefore, $\alpha\Delta p^1$ is the real Δp value. Here we used the linearized volume change for small $h(\theta)$,

$$\Delta V/V = 3\int_0^{\pi/2} h(\theta)\sin(\theta)\,d\theta + \mathcal{O}(h^2). \quad \text{(A2)}$$

APPENDIX B: CLEBSCH-GORDAN EXPRESSION FOR Γ_θ^{lm}

From the radiation pressure Eq. (3) and electric field Eq. (1) expressions, we can write the normalized pressure f_{lm} as

$$f_{lm} = \frac{|\vec{X}_{lm}|^2}{|\vec{X}_{lm}|^2_{\max}}. \tag{B1}$$

Note that the expression of Γ_θ^{lm} in Eq. (18) can be transformed into a surface integral,

$$\Gamma_\theta^{lm} = -\frac{n_{\rm co}a}{\lambda}\frac{1}{|\vec{X}_{lm}|^2_{\max}}\int_0^\pi |\vec{X}_{lm}|^2 Y_{20}(\theta)\sin(\theta)\,d\theta = -\frac{n_{\rm co}a}{2\pi\lambda}\frac{1}{|\vec{X}_{lm}|^2_{\max}}\iint |\vec{X}_{lm}|^2 Y_{20}\,d\Omega. \tag{B2}$$

With the Clebsch-Gordan expression for surface integral [39]

$$\iint |\vec{X}_{lm}|^2 Y_{LM}\,d\Omega = \left[1 - \frac{L(L+1)}{2l(l+1)}\right]\sqrt{\frac{2L+1}{4\pi}}\langle L,l;M,m|l,m\rangle\langle L,l;0,0|l,0\rangle, \tag{B3}$$

Eq. (19) can be obtained with $L = 2, M = 0$. Equation. (22) can also be obtained by Eq. (B3).

[1] V. B. Braginsky, Y. I. Vorontsov, and K. S. Thorne, Quantum nondemolition measurements, Science **209**, 547 (1980).

[2] F. Vollmer, D. Braun, A. Libchaber, M. Khoshsima, I. Teraoka, and S. Arnold, Protein detection by optical shift of a resonant microcavity, Appl. Phys. Lett. **80**, 4057 (2002).

[3] H. Zhu, I. M. White, J. D. Suter, P. S. Dale, and X. Fan, Analysis of biomolecule detection with optofluidic ring resonator sensors, Opt. Express **15**, 9139 (2007).

[4] P. A. Franken, A. E. Hill, C. W. Peters, and G. Weinreich, Generation of Optical Harmonics, Phys. Rev. Lett. **7**, 118 (1961).

[5] A. A. Savchenkov, A. B. Matsko, D. Strekalov, M. Mohageg, V. S. Ilchenko, and L. Maleki, Low Threshold Optical Oscillations in a Whispering Gallery Mode CaF_2 Resonator, Phys. Rev. Lett. **93**, 243905 (2004).

[6] J. U. Fürst, D. V. Strekalov, D. Elser, A. Aiello, U. L. Andersen, C. Marquardt, and G. Leuchs, Low-Threshold Optical Parametric Oscillations in a Whispering Gallery Mode Resonator, Phys. Rev. Lett. **105**, 263904 (2010).

[7] M. Hossein-Zadeh and K. J. Vahala, Fiber-taper coupling to whispering-gallery modes of fluidic resonators embedded in a liquid medium, Opt. Express **14**, 10800 (2006).

[8] A. Jonáš, Y. Karadag, M. Mestre, and A. Kiraz, Probing of ultrahigh optical q-factors of individual liquid microdroplets on superhydrophobic surfaces using tapered optical fiber waveguides, J. Opt. Soc. Am. **29**, 3240 (2012).

[9] Z. Li and D. Psaltis, Optofluidic dye lasers, Microfluid. Nanofluid. **4**, 145 (2007).

[10] U. Levy and R. Shamai, Tunable optofluidic devices, Microfluid. Nanofluid. **4**, 97 (2008).

[11] K. Sakai, D. Mizuno, and K. Takagi, Measurement of liquid surface properties by laser-induced surface deformation spectroscopy, Phys. Rev. E **63**, 046302 (2001).

[12] S. Mitani and K. Sakai, Measurement of ultralow interfacial tension with a laser interface manipulation technique, Phys. Rev. E **66**, 031604 (2002).

[13] R. Pobre and C. Saloma, Radiation force on a nonlinear microsphere by a tightly focused gaussian beam, Appl. Opt. **41**, 7694 (2002).

[14] H. Rokhsari, T. J. Kippenberg, T. Carmon, and K. J. Vahala, Theoretical and experimental study of radiation pressure-induced mechanical oscillations (parametric instability) in optical microcavities, IEEE J. Sel. Top. Quantum Electron. **12**, 96 (2006).

[15] T. J. Kippenberg and K. J. Vahala, Cavity opto-mechanics, Opt. Express **15**, 17172 (2007).

[16] T. J. Kippenberg and K. J. Vahala, Cavity optomechanics: Back-action at the mesoscale, Science **321**, 1172 (2008).

[17] A. Ashkin and J. M. Dziedzic, Radiation Pressure on a Free Liquid Surface, Phys. Rev. Lett. **30**, 139 (1973).

[18] I. Komissarovak, G. Ostrovskaya, and E. Shedova, Light pressure induced deformations of a free liquid surface, Opt. Commun. **66**, 15 (1988).

[19] H. M. Lai, P. T. Leung, K. L. Poon, and K. Young, Electrostrictive distortion of a micrometer-sized droplet by a laser pulse, J. Opt. Soc. Am. B **6**, 2430 (1989).

[20] A. Casner and J.-P. Delville, Adaptative lensing driven by the radiation pressure of a continuous-wave laser wave upon a near-critical liquid-liquid interface, Opt. Lett. **26**, 1418 (2001).

[21] A. Casner, J.-P. Delville, and I. Brevik, Asymmetric optical radiation pressure effects on liquid interfaces under intense illumination, J. Opt. Soc. Am. B **20**, 2355 (2003).

[22] E. Brasselet, R. Wunenburger, and J.-P. Delville, Liquid Optical Fibers with a Multistable Core Actuated by Light Radiation Pressure, Phys. Rev. Lett. **101**, 014501 (2008).

[23] J.-P. Delville, M. Robert de Saint Vincent, R. D. Schroll, H. Chraïbi, B. Issenmann, R. Wunenburger, D. Lasseux, W. W. Zhang, and E. Brasselet, Laser microfluidics: Fluid actuation by light, J. Opt. A: Pure Appl. Opt. **11**, 034015 (2009).

[24] H. Chraibi, R. Wunenburger, D. Lasseux, J. Petit, and J.-P. Delville, Eddies and interface deformations induced by optical streaming, J. Fluid Mech. **688**, 195 (2011).

[25] I. Brevik and R. Kluge, Oscillations of a water droplet illuminated by a linearly polarized laser pulse, J. Opt. Soc. Am. B **16**, 976 (1999).

[26] S. Å. Ellingsen, Microdroplet oscillations during optical pulling, Phys. Fluids **24**, 022002 (2012).

[27] S. Å. Ellingsen, Theory of microdroplet and microbubble deformation by gaussian laser beam, J. Opt. Soc. Am. B **30**, 1694 (2013).

[28] D. Tapp, J. M. Taylor, A. S. Lubansky, C. D. Bain, and B. Chakrabarti, Theoretical analysis for the optical deformation of emulsion droplets, Opt. Express **22**, 4523 (2014).

[29] Y. Xu, P. Zhang, S. Jung, and A. Lee, Analysis of radiation pressure induced nonlinear optofluidics, Opt. Express **22**, 28875 (2014).

[30] J. D. Jackson, *Classical Electrodynamics*, 3rd ed. (Wiley & Sons, New York, 1998).

[31] C. Pozrikidis, *Boundary Integral and Singularity Methods for Linearized Viscous Flow* (Cambridge University Press, Cambridge, UK, 1992).

[32] G. Graziani, A boundary integral equation method for axisymmetric viscous flows, Int. J. Eng. Sci. **27**, 855 (1989).

[33] A. Prosperetti and G. Tryggvason, *Computational methods for multiphase flow* (Cambridge University Press, Cambridge, UK, New York, 2007).

[34] H. Chraïbi, D. Lasseux, E. Arquis, R. Wunenburger, and J.-P. Delville, Simulation of an optically induced asymmetric deformation of a liquid-liquid interface, Eur. J. Mech. B: Fluids **27**, 419 (2008).

[35] R. W. Boyd, *Nonlinear Optics*, 3rd ed. (Academic, Amsterdam, 2008).

[36] M. A. Choma, A. K. Ellerbee, C. Yang, T. L. Creazzo, and J. A. Izatt, Spectral-domain phase microscopy, Opt. Lett. **30**, 1162 (2005).

[37] A. Lee, B. Zhang, C. Ma, A. Wang, and Y. Xu, Fiber-based white-light interferometry for nanoscale distance measurement and control, IEEE Photonics Technol. Lett. **24**, 2136 (2012).

[38] Z. Yu and A. Wang, Fast white light interferometry demodulation algorithm for low-finesse fabry-pérot sensors, IEEE Photonics Technology. Lett. **27**, 817 (2015).

[39] H. M. Lai, P. T. Leung, K. Young, P. W. Barber, and S. C. Hill, Time-independent perturbation for leaking electromagnetic modes in open systems with application to resonances in microdroplets, Phys. Rev. A **41**, 5187 (1990).

[40] V. R. Dantham, S. Holler, C. Barbre, D. Keng, V. Kolchenko, and S. Arnold, Label-free detection of single protein using a nanoplasmonic-photonic hybrid microcavity, Nano Lett. **13**, 3347 (2013).

[41] P. Than, L. Preziosi, D. Josephl, and M. Arney, Measurement of interfacial tension between immiscible liquids with the spinning road tensiometer, J. Colloid Interface Sci. **124**, 552 (1988).

[42] A. Datta, S. Kundu, M. K. Sanyal, J. Daillant, D. Luzet, C. Blot, and B. Struth, Dramatic enhancement of capillary wave fluctuations of a decorated water surface, Phys. Rev. E **71**, 041604 (2005).

[43] H. Chraïbi, D. Lasseux, R. Wunenburger, E. Arquis, and J.-P. Delville, Optohydrodynamics of soft fluid interfaces: optical and viscous nonlinear effects, Eur. Phys. J. E: Soft Matter Biol. Phys. **32**, 43 (2010).

[44] H. Leitão, A. M. Somoza, M. M. Telo da Gama, T. Sottmann, and R. Strey, Scaling of the interfacial tension of microemulsions: A phenomenological description, J. Chem. Phys. **105**, 2875 (1996).

[45] S. R. Palit, Thermodynamic interpretation of the eötvös constant, Nature (London) **177**, 1180 (1956).

[46] B. Davidovitch, E. Moro, and H. A. Stone, Spreading of Viscous Fluid Drops on a Solid Substrate Assisted by Thermal Fluctuations, Phys. Rev. Lett. **95**, 244505 (2005).

[47] K. Mecke and M. Rauscher, On thermal fluctuations in thin film flow, J. Phys.: Condens. Matter **17**, S3515 (2005).

[48] W. Brouwer and R. K. Pathria, On the surface tension of liquid helium ii, Phys. Rev. **163**, 200 (1967).